CHALMERS

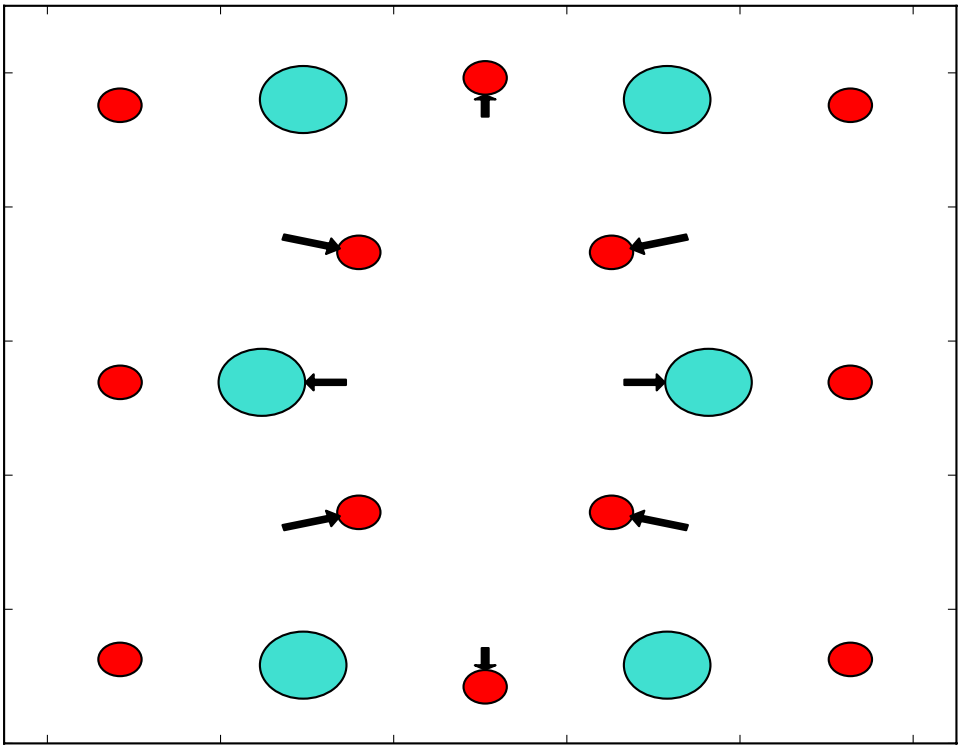

A Theoretical Study of Doping and the Hydration Process of Barium Zirconate

MAGNÚS ÞÓR BENEDIKTSSON

Department of Applied Physics
CHALMERS UNIVERSITY OF TECHNOLOGY
Gothenburg, Sweden 2013

Abstract

In this thesis we give a brief review of Kohn-Sham density functional theory and different exchange-correlation functionals. The $BaZrO_3$ lattice constant is obtained and the ground state considered. We examine the electronic structure using PBE and PBE0. PBE0 provides a greatly improved density of states. We consider the use of H_2O as a reference molecule for μ_O which reduces error due to PBE's description of O_2 binding energy by 40%. We compare the local environment around an oxygen vacancy in $BaZrO_3$ to that in $SrTiO_3$ and examine the expansion due to dopant atoms and hydration in $BaZrO_3$. Then follows a comparative study between the PBE and PBE0 description of oxidation and hydration in $BaZrO_3$. We calculate the reaction enthalpies, equilibrium rate constants and defect concentration profiles most relevant for the reactions. The PBE0 and PBE oxidation enthalpy are positive and negative respectively which leads to very different rate constants and concentration profiles. However, neither one of the enthalpies seem to contradict experimental evidence of increased electrical conductivity at elevated temperature.

Keywords: Barium Zirconate, DFT, PBE, PBE0, Hydration, Oxidation, Defect Concentration, Lattice Expansion.

Acknowledgements

I want to thank my supervisor, Göran Wahnström, for his guidance through this work. Anders Lindman for his code, calculations and assistance. Paul Erhart for his code. Edit Helgee for her assistance. My friends at Chalmers, my parents and Jóhanna for being there. Also you whom I have forgotten to mention.

This research was conducted using the resources of High Performance Computing Center North (HPC2N) and Chalmers Center for Computational Science and Engineering (C^3SE).

Contents

1 Introduction

Learning how to manipulate materials and developing new materials has been an important part of human history. Developments such as metallurgy, plastics, glass and many more are a large part of modern society and material science is truly one of the frontiers of modern technological advancement.

With the discovery of the atom and the development of quantum mechanics mankind has deepened its understanding of the structure of matter. With this knowledge dawned the possibility of predicting new materials with certain properties from calculations. For state of the art technology it is then possible to tailor make materials with appropriate properties, at least theoretically. This is important for developing electronic devices that require very specific properties.

Proton conducting metal oxides have many prospective technical applications such as electrolytes in fuel cells, gas sensors, batteries and hydrogen pumps. Perovskite materials have gained a lot of interest of late as proton conductors[1] and the emphasis of this thesis will be on the perovskite structured metal oxide $BaZrO_3$. $BaZrO_3$ shows very promising properties for a variety of possible applications such as wireless communications, a thin film substrate[2] a high chemical stability in CO_2 rich atmospheres[1][3][4], mechanical stability and high proton conductivity when doped[1][5]. In fact, $BaZrO_3$ has one of the highest bulk conductivity amongst the proton conducting perovskites[6] The mechanical and chemical stability of $BaZrO_3$ make it an attractive material as a solid oxide fuel cell (SOFC) electrolyte.

The theoretical tools to accurately predict the necessary properties of a given material have been readily available for decades but they have not been really practical without great computing power. Over the last thirty years computing capabilities have increased considerably and the development of computational tools to tackle this problem has moved forward. Even with these advances, computational burden remains an obstacle but one of the method that is more accessible to less powerful computers is density functional theory (DFT). DFT uses a self-consistent algorithm to converge on a electron density for an atomic system and is sufficiently accurate for many applications.

1.1 $BaZrO_3$

$BaZrO_3$ is a metal oxide with a fairly large band gap of 5.3 eV [7]. With one of the highest bulk conductivity compared with other proton conducting perovskites it makes a promising material for intermediate temperature electrolytes. $BaZrO_3$ possesses more enticing properties such as a mechanical and chemical stability that

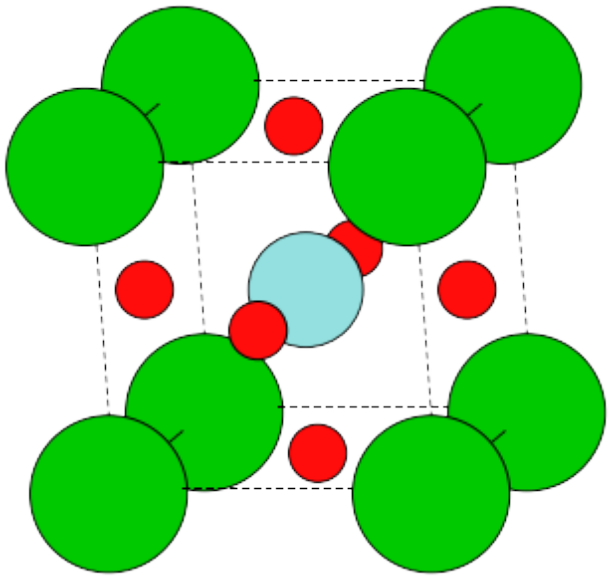

(a) The perfectly cubic perovskite structure.

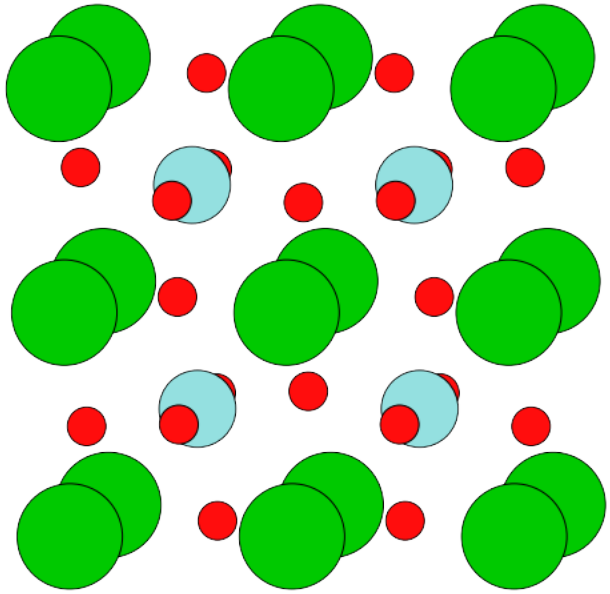

(b) In this figure we can see the ZrO_8 octahedra tilted slightly

Figure 1: The ground state perovskite structure of $BaZrO_3$, Barium: Green, Zirconium: Cyan, Oxygen: Red. Whether the ground state is perfectly cubic (figure 1a) or if the ZrO_6 octahedra are tilted (figure1b) is debated.

are convenient for any electrolyte meant for small vehicles.

Despite the promises of $BaZrO_3$, it has it's drawbacks. High impedance at the grain boundaries poses a problem[4][8] and some fundamental aspects are not fully known.

The ground state structure is fairly debated. Most experimental reports assign $BaZrO_3$ a perfectly cubic structure (figure 1a) while the bulk of ab-initio DFT studies report the cubic structure unstable with regard to an octahedral tilt([9] and within) as in figure 1b. These tilts could be present without showing up in experiments since the mean positions of the oxygens are the same for the cubic and theoretically tilted system.

Conductivity in $BaZrO_3$ is related to the concentration of hydrogen within the system. The material is hydrated by filling oxygen vacancies. To increase conductivity the material is usually doped by substituting some of the Zr^{4+} with a trivalent dopant M^{3+}. This results in an increased number of oxygen vacancies compensating for the charge difference. For every two dopant atoms included one oxygen vacancy is formed which allows for increased hydrogen concentration. During this process the material expands and care must be taken so that it does not crack. This is important as protons can not diffuse across cracks. Results from a recent study by Yamazaki et al.[10] show that there is evidence for oxidation reaction occurring along side the hydration process which creates unwanted electron holes within the material.

1.2 Thesis outline

First we give a description on the theoretical tools applied in the thesis. In section 2 we give a short review of Khon-Sham DFT and different exchange-correlation approximations as well as the practical methods used to solve the theoretical problem using a computer. Section 3 introduces models used to investigate the properties of $BaZrO_3$ in the results section of this thesis.

Some different approximation are applied to examine some ground state properties of $BaZrO_3$, stability phases, electronic structure and crystal structure. The theoretical models from section 3 are then applied to investigate the effects of dopants and hydration on the structure of $BaZrO_3$ using DFT. We examine the local environment surrounding oxygen vacancies in $BaZrO_3$ more closely and consider the relationship between the local environment effects on the large scale structure. Finally we consider the efficiency of the hydration process with respect to other possible processes.

2 DFT

2.1 The adiabatic approximation

With DFT one makes use of the adiabatic approximation by Born and Oppenheimer [11]. In an atomic system electronic forces govern and as the nuclei are massive in comparison to the electrons they respond to the forces with greater inertia. We can then safely assume that the electrons manage to remain in their ground state configuration relative to the nuclei positions while the nuclei move according to the forces. This is convenient for computer simulations where we are constricted to discrete time. At each point in time we keep the nuclei positions fixed while we derive the electron density of the system with the static potential created by the nuclei. From this we calculate the forces acting on each nuclei and move them accordingly. This is iterated until the forces on the nuclei are vanishing and we arrive at a ground state configuration for the system. This effectively reduces the problem of finding the ground state of the whole system to just looking at the electronic system.

2.2 Hohenberg and Kohn

Even with the nuclei out of the picture solving the electronic system is a formidable task. The base for a solution was built by Hohenberg and Kohn in 1964 [12] when they demonstrated that an external potential $v(\mathbf{r})$ of a system of electrons is a unique functional of the ground state electron density $n(\mathbf{r})$. Since the system hamiltonian is a functional of $v(\mathbf{r})$ the ground state wave function Ψ is uniquely determined by $n(\mathbf{r})$ and so are all ground state electronic properties.

They went on to show that the functional

$$E_v[n] = \int v(\mathbf{r})n(\mathbf{r})d\mathbf{r} + F[n]$$

is minimized by the ground state density $n(\mathbf{r})$ and the resulting minimum value equals the ground state energy. The universal functional $F[n] = \langle\Psi|\,\hat{T}+\hat{U}\,|\Psi\rangle$ is the kinetic and electron-electron interaction part of the energy independent of $v(\mathbf{r})$.

2.3 Kohn and Sham

Kohn and Sham [13] brought the Hohenberg-Kohn DFT to practicality by realizing a connection between the system of interacting electrons to a non-interacting one.

They replaced the problem of the interacting system of $v(\mathbf{r})$ with a non-interacting system of $v(\mathbf{r})$ with an error term. They wrote

$$E_{KS}[n] = \int v(\mathbf{r})n(\mathbf{r})d\mathbf{r} + T_s[n] + E_h[n] + E_{xc}[n]$$

with $T_s[n]$ as the kinetic energy of the non-interacting electron system and $E_h[n]$ as the electrostatic Hartree term. The last term is where Kohn and Sham have gathered the difficult exchange and correlation parts of the energy. If $E_{xc}[n] = \int n(\mathbf{r})\epsilon_{xc}[n(\mathbf{r})]d\mathbf{r}$, we arrive at the so called Kohn-Sham equations by minimizing with respect to the density:

$$\left[-\frac{1}{2}\nabla^2 + V_{KS}\right]\psi_i = \epsilon_i\psi_i$$

From the solutions of these equations we construct an electron density

$$n = \sum_i^N |\psi_i|^2$$

where N is the number of electrons in the system and i goes up from the lowest eigenvalue orbital ψ_i. We now have a solution for E_{KS}. From an initial guess for the density we calculate $V_{KS} = v(r) + V_h + V_{xc}$ which we use to find the KS-orbitals ψ_i and construct a new density. This process is then iterated until a self-consistent density is reached.

So what has effectively been done is to change the problem of solving an interacting electron system to a problem of solving non-interacting electrons moving in an effective potential. The V_{xc} is then the part of the potential that covers the many-body effects but even with this progress we still have no explicit expression for V_{xc}.

2.4 Exchange correlation functionals

In order to be able to do the iteration process described above we need an approximation for E_{xc}. Many such exist but here we will discuss only the most simple one and then the two that are applied in the thesis.

The simplest functional, presented by [13], is the local density approximation (LDA) where the xc-functional at each point in space is only dependent on the electron density at that precise point.

$$E_{xc}^{LSD}[n] = \int d^3r\, n(r)\epsilon_{xc}^{hom}(n(r))$$

More accurately the exchange-correlation energy per electron is approximated by the that of homogeneous electron gas which has a known simple analytical form for the exchange part. The high and low density limits of the correlation part are known analytically. Data from ref. [14] for the density can be interpolated in order to construct a description for the intermediate values of the density. Theoretically this approximation should be appropriate for systems with a near to homogeneous electron density such as certain solids and naturally worse for isolated molecules and atoms where the density is not as uniform.

2.4.1 PBE, a GGA

To better describe a system with a varying density it seems natural to include information about the gradient of the density at each point in space as well the density it self. A class of such functionals are the Generalized gradient approximations (GGA). Usually only the first derivatives are included since any higher terms do not necessarily refine the approximation but on the contrary some times make it worse.

$$E_{xc}^{GGA}[n] = \int d^3r f(n, \nabla n)$$

There exists an abundance of different GGA's, empirical, semi-empirical [15][16][17]. The one used in this thesis is named PBE after Perdew, Burke and Ernzerhof introduced in 1996[18] and is one of the most widely used GGA amongst physicists.[19][20]

The correlation part is the same as in LDA plus a correction term that includes the gradient of the density

$$E_c^{GGA}[n] = \int d^3r\, n\big[\epsilon_c^{hom}(r_s) + H(r_s, t)\big]$$

and the exchange part is written in the same manner as all GGA's

$$E_x^{GGA}[n] = \int d^3r\, n\epsilon_x^{hom}(n)F_x(s)$$

Here the variables t and s are two different dimensionless density gradients $\sim |\nabla n|/n$. The correction term H and the factor F are chosen such that certain limiting conditions on the exchange and correlation energy densities are fulfilled. The explicit forms of these are not very illuminating but the main idea behind PBE is to construct them with all parameters as fundamental constants and not fitted to empirical

data. The conditions on the densities were chosen in such a way that the resulting functional reproduces the correct behavior of LDA and the most relevant features from numerical GGA calculations.[18][21]

A common fault of GGA's and specifically of PBE is that it systematically underestimates the band gap[22][23][24] and the atomization energies of multiply bonded molecules[25] which can be improved upon as we see in the next section.

2.4.2 PBE0, a hybrid functional

It is possible to calculate the exact Hartree exchange energy from Kohn-Sham orbitals[13] and in 1993(1992) Becke[26] argued why it would be proper to use a part of the exact energy in mixture with the DFT approximated energy. It can be shown [26][27] that the exchange energy can be written

$$E_{xc} = \int_0^1 U_{xc}^{\lambda} d\lambda$$

This is the adiabatic connection formula which connects the fully interacting electronic system ($\lambda = 1$) to the non-interacting one ($\lambda = 0$) through a continuous set of partially interacting systems with a coupling strength parameter λ. A natural first-approximation of the integral would be the mean value of the end points $E_{xc} \approx 0.5(U_{xc}^1 + U_{xc}^0)$, the so called half and half functional. As U_{xc}^0 is just the exact Hartree exchange which can be evaluated without approximation it seems proper to do so. Taking this idea further Becke constructed the following functional

$$E_{xc} = E_{xc}^{LDA} + a_0\big(E_x^{exact} - E_x^{LDA}\big) + a_x\big(E_{xc}^{GGA} - E_x^{LDA}\big) + a_c\big(E_c^{GGA} - E_c^{LDA}\big)$$

where he fitted the coefficients a_0, a_x and a_c to experimental data. This functional greatly improved upon the accuracy of prior DFT methods (LDA and GGA) and rivaled more accurate contemporary quantum thermochemistry methods. Later he [28] presented a simplified functional with $a_x = 1 - a_0$ and $a_c = 1$ resulting in

$$E_{xc} = E_{xc}^{DFT} + a_0\big(E_x^{exact} - E_x^{DFT}\big)$$

This provided even better results than the three parameter hybrid.

In the spirit of the PBE GGA, Perdew, Burke and Ernzerhof provided a value for a_0 through qualitative physical reasoning rather than fitting to experimental data.[29] They showed that $a_0 = 0.25$ which was close to the fitted value 0.28 found in [28] and this functional is shown to perform remarkably well compared to more heavily fitted methods.[30][20] This functional is called PBE0.

2.5 Solution in practice

In order to solve the Kohn-Sham equations in practice we expand the single particle wave functions, ψ_i's, in some basis. This transforms the problematic differential equations into a linear eigenvalue problem. This method provides an easy way to tune the precision of calculations as a large basis set is able to describe the wave function more accurately than a small one. The computational effort also increases with the size of the basis set so one would optimally want to use the smallest possible basis set to reach the desired accuracy.

There exists a variety of different basis sets to choose from. The linear combination of atomic orbitals (LCAO) consists of localized functions most often centered on the atomic positions. Subcategories of this method would be the slater-type orbitals (STO) and Gaussian-type orbitals (GTO) basis sets which respectively use slater orbitals and gaussians as basis functions as the names indicate. Although the GTO requires a larger set of functions, all but the exchange-correlation matrix elements can be obtained analytically which makes it faster than the STO.

It is important to choose a suitable basis for the problem at hand. The LCAO's are more naturally applied to localized systems of atoms or molecules than to bulk materials. In systems with periodic boundary conditions like bulk systems it is usually more appropriate to apply Bloch's theorem[31] to expand the ψ_i's in a plane wave basis

$$\psi_j(r) = \sum_k c_j(k) e^{ikr}$$

The size of the plane wave basis is controlled by an energy cut off k_{max} which denotes the highest wave vector included in the basis set.

Many atomic potentials cause the wave function to fluctuate rapidly near the nuclei and the inner electrons. Describing these fluctuations in with a plane wave basis requires an enormous plane wave basis which makes the calculations rather time consuming. This is why a plane wave basis is usually applied in addition to so called pseudo potentials (PP) in stead of real atomic potentials. The idea of PP's is based on the observation that the innermost electrons rarely participate in electrochemical bonding between atoms. The PP's mimic the atomic potentials exactly down to a given cut off radius. Within that region the atomic potential is replaced with a potential, with the same scattering properties, such that the resulting pseudo wave function is smooth and more easily represented in a plane wave basis.

These methods are readily available in various simulation software packages. The one used in this thesis is VASP[32], specifically version 5.2.12.

3 Theoretical Modeling

3.1 Hydration and oxidation of $BaZrO_3$

The reaction presumed to be responsible for the hydration of doped $BaZrO_3$ is the so called filling the oxygen vacancies:

$$\mathrm{V_O^{\cdot\cdot}} + \mathrm{O_O} + \mathrm{H_2O(g)} \leftrightarrow 2\mathrm{OH_O^{\cdot}} \tag{1}$$

Through this reaction the amount of hydrogen absorbed is related to the vacancy concentration. In order to increase the proton conductivity which is proportional to the number of charge carriers, $BaZrO_3$ is doped by substituting some of the Zr^{4+} with a trivalent dopant M^{3+}, Y^{3+} for instance. The net result is an increased concentration of oxygen vacancies compensating the charge difference. The vacancies are +2 while the the relative charge of the dopants is -1 so ideally one vacancy forms per every two dopant atoms. This however is not the only possible way to fill the vacancies. In dry atmospheric conditions the material oxidizes through

$$\frac{1}{2}\mathrm{O_2(g)} + \mathrm{V_O^{\cdot\cdot}} \leftrightarrow \mathrm{O_O} + 2\mathrm{h^{\cdot}} \tag{2}$$

Under wet conditions it would then be possible for water based oxidation

$$\mathrm{H_2O(g)} + \mathrm{V_O^{\cdot\cdot}} \leftrightarrow \mathrm{O_O} + 2\mathrm{h^{\cdot}} + \mathrm{H_2}$$

to occur since the humid atmosphere must be an equilibrium between H_2O, H_2 and O_2. A first approximation of the reaction enthalpies is just the total energy difference between the products and the reactants

$$\Delta H = \Delta E - p\Delta V = E^{tot}_{products} - E^{tot}_{reactants} \tag{3}$$

since the DFT calculations are done at $p = 0$ and $T = 0$. This means that our material can have holes and conduct electricity which we usually do not want in applications. Whether this creates a problem depends on the hole conductivity vs. the proton conductivity of our material.

3.2 Formation energies and equilibrium rate constants

We define the formation energy of defects as the total energy difference between the pure system and the one with a defect introduced. For example, this is the formation energy of a vacancy V_O^q of charge q, calculated using a supercell of n primitive cells

$$\Delta E^f_{V_O^q} = E[n(\mathrm{BaZrO_{3-1/n}}); q] - E[n(\mathrm{BaZrO_3})] + \mu_{\mathrm{O}} + \mathrm{q}\mu_{\mathrm{e}} \tag{4}$$

The energy is of course dependent on the chemical potentials of the species we remove or add to the system when creating the defect. Similarly the formation energy of incorporating a proton into $BaZrO_3$ is

$$\Delta E^f_{H^q} = E[n(\mathrm{BaZrO_3H_{1/n}}); q] - E[n(\mathrm{BaZrO_3})] - \mu_{\mathrm{H}} + \mathrm{q}\mu_{\mathrm{e}} \tag{5}$$

The periodic boundary condition of the supercell used in practice means that there will inevitably be interaction between defects unless a large enough cell is used. A larger cell requires more computing power and which makes it unattractive. However, [33] have estimated the coulombic error in total energy due to interactions of charged defects in periodic system with a period L, defect charge q and ε the macroscopic dielectric constant of the medium the defects are embedded in. Their estimate is

$$E_{\mathrm{error}} = -\frac{\alpha q^2}{2\varepsilon L}$$

which we have then subtracted from all total energies.

In order to examine the competition between oxidation and hydration in the material we must calculate the equilibrium rate constants for the reactions

$$K = \exp\left(-\frac{\Delta G^f}{k_B T}\right) \tag{6}$$

The Gibbs free energy

$$G(p,T) = H(p,T) - TS(p,T) \tag{7}$$

can be approximated for the solid phases as the vibrational part of the free energy added to the total electronic energy

$$G(p,T) = E^{tot} + F^{vib}(T)$$

with

$$F^{vib}(T) = \sum_{s=1}^{3N} \frac{h\nu_s}{2} + k_B T \ln\left[1 - \exp\left(-h\nu_s / K_B T\right)\right]$$

The sum adds the contributions from all normal modes in a lattice containing N atoms. For the reactions the Gibbs energy change becomes

$$\Delta G^f = \Delta E^{tot} + \Delta \tilde{G}^{vib}(T) + \Delta G^{vib}(T) + \Delta G^{gas}(p,T) \tag{8}$$

as described thoroughly by [34]. For hydration we have $\Delta E^{tot} = 2\Delta E^f_{H^+} - \Delta E^f_{V_O^{2+}}$ which is the change in electronic energy caused by creating two protonic defects and

filling a vacancy. $\Delta\tilde{G}^{vib}(T)$ are the contributions from the three atoms added to the system. By adding three new atoms we've introduced 3×3 new normal modes to the lattice. The $\Delta G^{vib}(T)$ contains the contributions due to the altered vibrational frequencies of the nearest neighbour atoms coordinated with the added atoms. The oxidation on the other hand has $\Delta E^{tot} = -\Delta E^{f}_{V_O^{2+}}$ and the solid vibrational parts obviously do not include effects from protons. Finally the last term describes the free energy change when a water or an oxygen molecule is lost from the gas phase at partial pressure p

$$\Delta G^{gas}_{H_2O/O_2}(p,T) = -h^0(T) + Ts^0(T) - k_B T \ln \frac{p}{p^0}$$

Treating the oxidation reaction in this way to calculate the rate constant is technically incorrect. The holes should not be treated as defects occupying localized sites but as band states occupying energy levels which leads to a different rate constant. However, the two distinct rate constants are related through

$$K_{defects} = \frac{p_{H_2O} c_{V_O^{2+}}}{n_h^2} K_{band\,states}$$

with $c_{V_O^{2+}}$ and n_h defined as in the next section. Because of this simple relation we'll treat the holes as defects in our results.

3.3 Defect concentrations, charge neutrality and the electron chemical potential

Using the formation energies we can calculate the temperature dependent defect concentration

$$c_{def} = c^0_{def} \exp\left(-\frac{\Delta G^f_{def}(p,T)}{k_B T}\right) \tag{9}$$

c^0_{def} is the site density for the specific defect, i.e. number of sites to form a defect per volume. The atomic chemical potentials can be calculated or tuned to represent different chemical environments but the electron chemical potential, μ_e is more difficult to pinpoint. μ_e is dependent on the densities of charge carriers and dopants through the charge neutrality condition which states that for a charge neutral material the total charge of all charge carriers and charged defects must cancel out

$$\sum_i q_i c_i + n_h - n_e = 0 \tag{10}$$

The sum runs over all possible point defects and their charge states, n_h and n_e are the concentration of holes in the valence band and electrons in the conduction band respectively. In practice it is of course impossible to include all possible defects so an approximation must be made to which defects are relevant. Take for example yttrium doped $BaZrO_3$, our charge neutrality becomes at first approximation

$$-c_{Y_{Zr}} + n_h - n_e = 0$$

but as discussed in section 1.1, the doping induces a charged oxygen vacancy per every two dopant atoms which can not be neglected so we need to include the vacancies

$$-c_{Y_{Zr}} + 2c_{V_O^{2+}} + n_h - n_e = 0$$

One might want to add to this dopant atoms placed on Ba sites and other possible defects but in this work we will include only these.

From basic solid state physics we know that the average number of electrons with a specific energy is

$$\bar{n}(\epsilon) = g(\epsilon)f(\epsilon, \mu_e) = g(\epsilon)(1 + \exp[(\epsilon - \mu_e)/\beta])^{-1}$$

where $g(\epsilon)$ is the density of states and $\beta = k_B T$.[35] The Fermi-Dirac distribution $f(\epsilon, \mu_e)$ represents the distribution of occupied states in the system so integrating this expression from the CBM to infinity gives us the concentration of charge carrying electrons in the conduction band.

$$n_e(\mu_e) = \int_{CBM}^{\infty} dE\ g(E)f(E, \mu_e)$$

Similarly we use the distribution of unoccupied states in the valence band to find the concentration of holes

$$n_h(\mu_e) = \int_{\infty}^{VBM} dE\ g(E)[1 - f(E, \mu_e)]$$

The equations above can be used to pinpoint the electron chemical potential. This has to be done self consistently as the charge neutrality equation has in general no analytical solution with the integral formulas for the carrier concentrations. From an initial guess for the electron chemical potential we can acquire values for the charge carrier concentrations and then solve for a new μ_e from the defect concentrations (eq. 9).

3.4 The band gap

The band gap is the difference in energies it takes to add one electron to a system and to remove one, i.e. the electron affinity and the ionization energy:

$$E_{gap} = E_A - E_I$$

This is in practice

$$\begin{aligned} E_{gap} &= (E^- - E) - (E - E^+) \\ &= E_{CBM} - E_{VBM} \end{aligned} \tag{11}$$

Where E_{CBM} and E_{VBM} are the conduction band minimum and valence band maximum respectively. A known problem of DFT is the band gap, GGA's tend to underestimate the band gap significantly and LDA's are no better. In order to calculate a more accurate band gap we can apply hybrid functionals which have been shown to improve it substantially.[36]

3.5 Formation volume

The way we calculate the formation volume of defects is similar to the partial molar volume of simple mixtures[37],

$$V_i = \left(\frac{\partial V}{\partial n_i}\right)_{p,T,n_{j\neq i}}$$

is the variation in the total volume of a solution with respect to the amount of substance i in that solution, while all other quantities are kept fixed. They partial molar volume of a substance depends on the composition of the solution because the molecular environment changes with the composition which affects the packing capability of the solution.

Our defect formation volume has to be defined at certain compositions as well. At high concentrations the defects interact more than under dilute conditions so it only makes sense to speak about a formation volume of a defect with respect to the concentration c.

However we cannot vary the concentration as easily as with a solution and see how the volume changes. We calculate the volume of the system with a certain concentration of defects and subtract the volume of the pure system

$$V_i^f = V_{defect}^{tot}(c_i = x) - V_{pure}^{tot}(c_i = 0)$$

This describes an infinite system through the periodic boundary conditions so theoretically adding one extra defect to this system will change the volume negligibly

since the concentration is essentially constant. The periodicity also means that we cannot add just one defect rather we add an infinite number of defects to an infinite system. We can think of the total volume change from the pure system to the defected one as the combined formation volume of all the defects at this concentration. In practice we use a super cell containing one or more defects. The volume change from the pure supercell to the defected one should account for the formation volume per the number of defects contained in the super cell at this specific concentration.

4 Results

4.1 Pure $BaZrO_3$

4.1.1 Atomic structure

We first determined the lattice parameter a, of cubic $BaZrO_3$ by relaxing a cubic unit cell containing five atoms. We used VASP and the GGA functional PBE with the PAW potentials released April 2012. The obtained value $a = 4.23$ Å is closer to the experimental value 4.19 Å[38] than 4.24-4.25 Å from prior PBE calculations using VASP[39] and SIESTA[9]. This is in line with the statement that the new PAW potential from April 2012 should improve the lattice constants of many oxides.

We compared the cubic system to the tilted octahedra system (figure 1) and found the cubic system to be energetically favorable by 10^{-3} eV. This is similar to the results of [40] and [41] where the energies of the two possible ground states are found similar with ab initio methods. Maier et al.[42] reported some local distortions within pure $BaZrO_3$ using Raman spectroscopy while their HRXRD shows a perfect cubic system. They suggest that their Raman results indicate an octahedral tilting. The fact that XRD does not detect tilted octahedra is likely to be caused by the mean value nature of XRD. If the system contains tilted octahedra it the macroscopic sample has them tilted in all directions so that the average position of the oxygen atoms will still be located at the undisturbed site. With the two structures so close in energies the system is likely to possess both phases though not coherently.[42]

Many theoretical studies address the issue ([43][41] and references within [9]) with different results on whether or not the ground state is perfectly cubic or not. Bilić and Gale[9] tried to sort out these differences by comparing multiple DFT implementations, potentials and functionals. Their conclusion is that the cubic lattice is indeed dynamically unstable but were unable to resolve the ground state. They predict that the instability induces tilting.

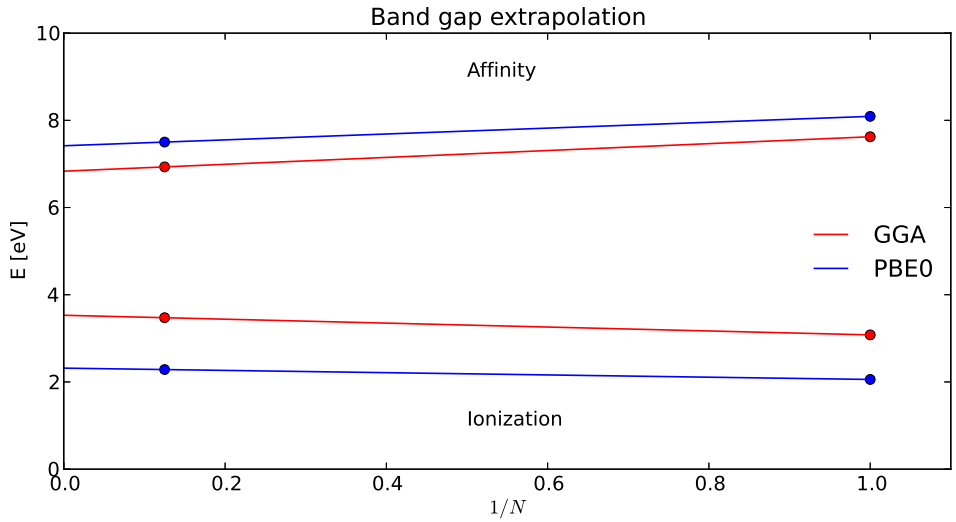

Figure 2: The extrapolated affinity and ionization energy. Here N is the number of unit cells in the supercell used to calculate the energies. We see a wider band gap given by PBE0 which is much more like the experimental value.

4.1.2 Electronic structure

We have also investigated the electronic structure of $BaZrO_3$. The band gap was calculated according to equation 11. In order to calculate correct E_{CBM} and E_{VBM} we add and remove electrons from different supercell sizes (1x1x1 and 2x2x2 unit cells) and extrapolate to the dilute limit, see figure 2. The values obtained from the extrapolation are given in table 1.

Oxide	PBE	PBE0	Experiment
ΔE_{gap}[eV]	3.3	5.1	5.3[7]

Table 1: $BaZrO_3$ band gap. The affinity and ionization energies have been extrapolated to reveal the band gap. We see a drastic improvement with the hybrid functional.

In figure 3 we examine the band gap of the DOS. There is a notable difference between the GGA and hybrid functional. Both the conduction band and the valence band shift to make the gap wider. The valence band shifts a little more than the conduction band. Looking at the edges of the band gap we notice that with higher resolution the gap could be broader than realized here. The whole DOS are depicted

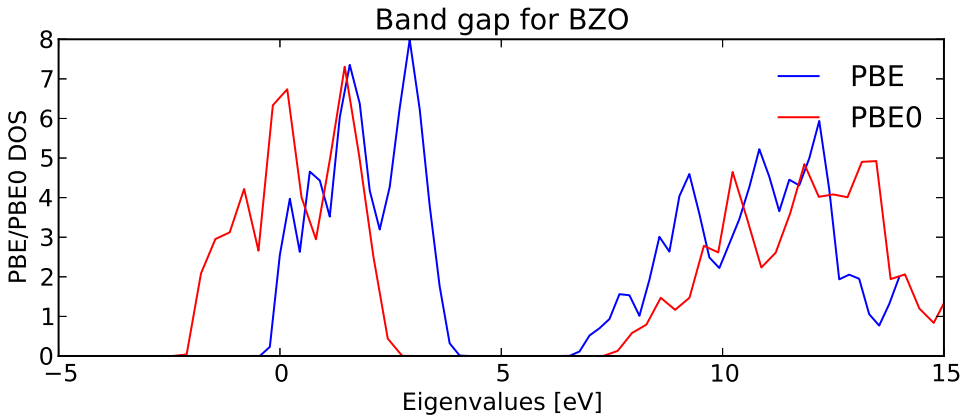

Figure 3: DOS around the band gap. The valence band and conduction band are seen shift lower down and higher up in energies respectively when we switch from PBE to PBE0. The valence band shifts a bit more than the conduction band.

in figure 4. The change is both a shift in accordance with the altered band gap (noticeable in all peaks below the valence band) and an overall dampening and broadening of the peaks most noticeable in the second peak close to -24 eV. We also note the large difference high in the conduction band. In figure 5 we see the calculated PBE band structure.

4.1.3 Formation energy

We've calculated the formation energies for $BaZrO_3$, ZrO_2, BaO and BaO_2 from their constituents: Ba_{bcc}, Zr_{hcp} and O_2 (table 3). In figure 6 we've plotted the calculated chemical stability range of $BaZrO_3$ from the formation energies. The triangle is defined by the individual chemical potentials adding up to the formation energy of $BaZrO_3$ or

$$\Delta\mu_{Ba} + \Delta\mu_{Zr} + 3\Delta\mu_O = \Delta H_f[\mathrm{BaZrO_3}]$$

and the contour within the triangle denotes equilibrium between $BaZrO_3$ and other possible oxide phases

$$\begin{aligned} \Delta\mu_{Ba} + \Delta\mu_O &= \Delta H_f[\mathrm{BaO}] \\ \Delta\mu_{Zr} + 2\Delta\mu_O &= \Delta H_f[\mathrm{ZrO_2}] \\ \Delta\mu_{Ba} + 2\Delta\mu_O &= \Delta H_f[\mathrm{BaO_2}] \end{aligned} \tag{12}$$

Our calculations underestimate the heats of formation. The reason for this could be the chemical potential μ_O. The PBE functional (GGA in general) is known

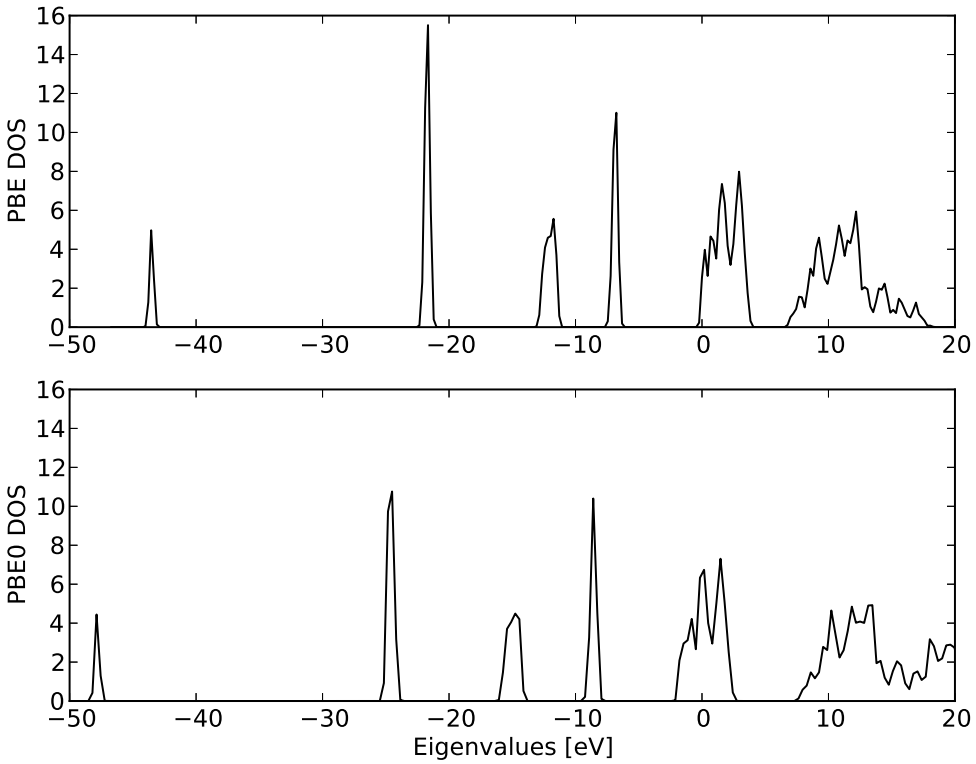

Figure 4: DOS. The DOS dampens and broadens a little as we switch from PBE to PBE0. We also note the overall lowering of eigenvalues of peaks below and in the valence band using PBE0 with respect to PBE0. The band gap widens and the upper end of conduction band changes considerably.

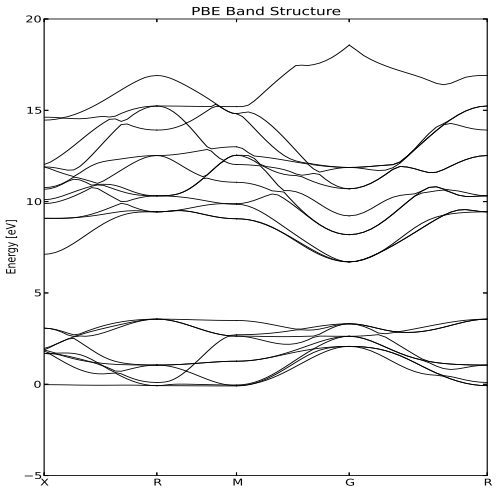

Figure 5: The PBE electronic band structure of $BaZrO_3$.

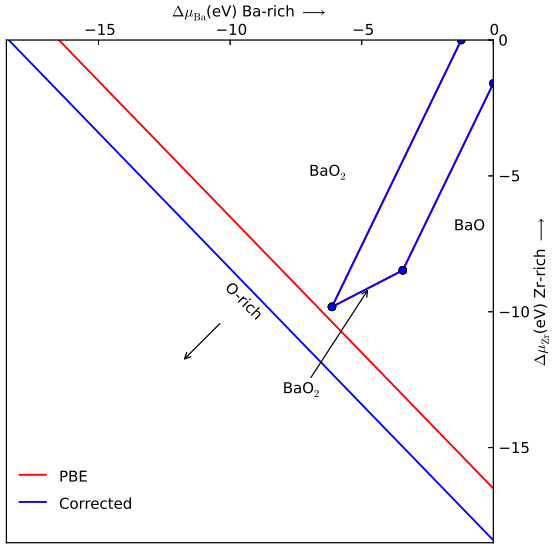

Figure 6: Chemical stability range of $BaZrO_3$. The red lines are calculated using the PBE total energies. The blue lines have their $E^{tot}[O_2]$ shifted by the error between PBE and experimental binding energy of the O_2 molecule. The boarders between $BaZrO_3$ and the other phases are unaffected by this.

to over estimate the binding energy of the molecule[25] resulting in a lower total energy for the molecule. Then $\mu_{\mathrm{O}} = \frac{1}{2}E_{tot}[\mathrm{O_2}]$ will be underestimated. Our current calculations overestimate the binding energy by 1.27 eV compared with the value from [25] lowering our potential by 0.635 eV. This difference offsets our heats of formation for $BaZrO_3$, ZrO_2, BaO and BaO_2 derived from this potential. If we correct for this difference we arrive much closer to the experimental values (table 3) which suggests that the oxygen chemical potential is responsible for greater part of the discrepancy between the experimental values and those calculated here. Using the experimental value for μ_{O} alters the chemical stability range as well. We see a clear shift in the diagonal line representing $\Delta\mu_{\mathrm{O}} = 0$, however the borders between $BaZrO_3$ and the other oxide phases remain intact as the shift of $\Delta\mu_{\mathrm{O}}$ cancels out in the calculation of eq. 12.

	O_2	H_2O	H_2	OH
Exact[eV]	5.22	10.07	4.75	4.61
PBE[eV]	6.23	10.16	4.54	4.76

Table 2: Discrepancies between PBE and experimental values of binding energies of molecules containing oxygen and hydrogen from ref. [25].

Instead of this semi-empirical approach we could use another reference for μ_O than the poorly described O_2. In reference [44] the author suggests using a water molecule and a hydrogen molecule since the binding energies of these molecules are more accurately described by PBE than O_2 as we see in table 2. This leads to

$$\begin{aligned} \mu_O &= E^{pbe}_{tot}[\mathrm{H_2O}] - E^{pbe}_{tot}[\mathrm{H_2}] \\ &= E^{ex}_{tot}[\mathrm{H_2O}] - 0.09 - (E^{ex}_{tot}[\mathrm{H_2}] + 0.21) \\ &= E^{ex}_{tot}[\mathrm{H_2O}] - E^{ex}_{tot}[\mathrm{H_2}] - 0.30 \end{aligned}$$

by using values from table 2 μ_O is underestimated by 0.5 eV using O_2. Considering more possibilities from the table from ref. [25] we managed to get the underestimation down to 0.255 eV using the molecules OH and H_2. Although this gets us closer to the experimental value it is not a drastic improvement but it gives the possibility of doing a more accurate purely theoretical approach than using O_2 as a reference.

4.2 Oxygen vacancies and lattice expansion

We calculated the formation energies, lattice constants and partial molar volumes for oxygen vacancies (table 4) for different concentrations and charge states. In figure 7

Oxide	PBE	Corrected	Experiment
$BaZrO_3$	-16.5	-18.4	-18.102[a]
BaO	-4.97	-5.6	-5.663[b]
ZrO_2	-10.2	-11.5	-11.309[b]
BaO_2	-6.5	-7.8	-

a: Ref. [45], *b*: Ref. [46]

Table 3: Heats of formation. Calculated values from PBE and the values with a correction to the oxygen chemical potential due to an overestimation of the O_2 binding energy. The corrected values are much closer to the experimental value than the purely PBE ones which implies that much of the error can be explained by the overestimated binding energy of O_2.

we see the formation energy (equation 4) as a function of μ_e within the band gap, where $\mu_e = 0$ has been shifted to the top of the valence band. By introducing a vacancy, the system reduces it's volume and according to table 4 we see that higher concentrations of vacancies reduce the volume even further.

	a_1[Å]	a_2[Å]	a_3[Å]	ΔV
V_O^{2+}(c=1/81)	4.227	4.220	4.220	-18.50
V_O(c=1/81)	4.236	4.234	4.234	0.04
$3V_O^{2+}$(c=3/81)	4.201	4.201	4.201	-16.08
V_O^{2+}(c=1/24)	4.209	4.186	4.186	-17.78

Table 4: Lattice constants of the system including a vacancy. a_{1-3} are orthogonal to each other and a_1 is parallel to a Zr-V_O-Zr bond. There are three possible orientations for the vacancy and thus the lattice constant is not the same in all directions. In the case of three vacancies in a 27 primitive cells, the constants reduce symmetrically since the vacancies are placed equidistant and each with a different orientation. ΔV is the change in volume the system exhibits divided by the number of vacancies in the system.

In order to describe the shape of the deformation caused by the vacancy we calculated the relaxation volume tensor[47]

$$\mathbf{v}^{rel} = \det(\mathbf{L}_0)\ln(\mathbf{L}_0^{-1}\mathbf{L}) \approx \det(\mathbf{L}_0)\mathbf{L}_0^{-1}(\mathbf{L}-\mathbf{L}_0)$$

where $\mathbf{L}$ and $\mathbf{L}_0$ are matrices of the supercell dimensions after and prior to the

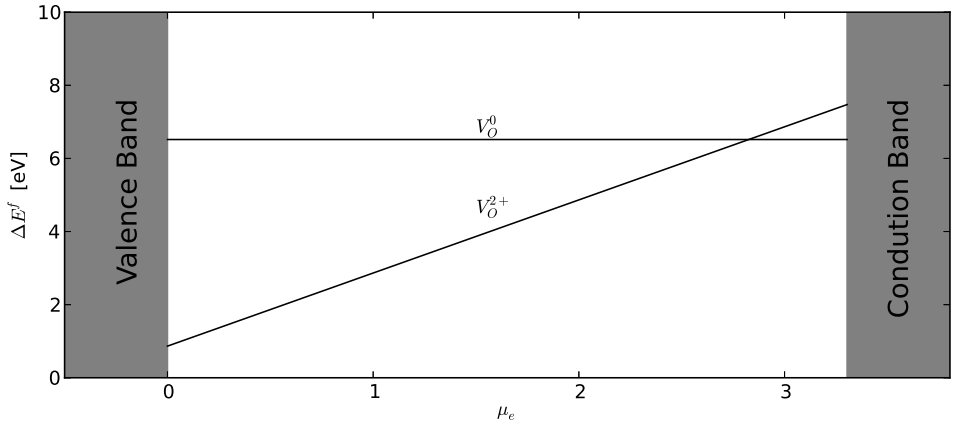

(a)

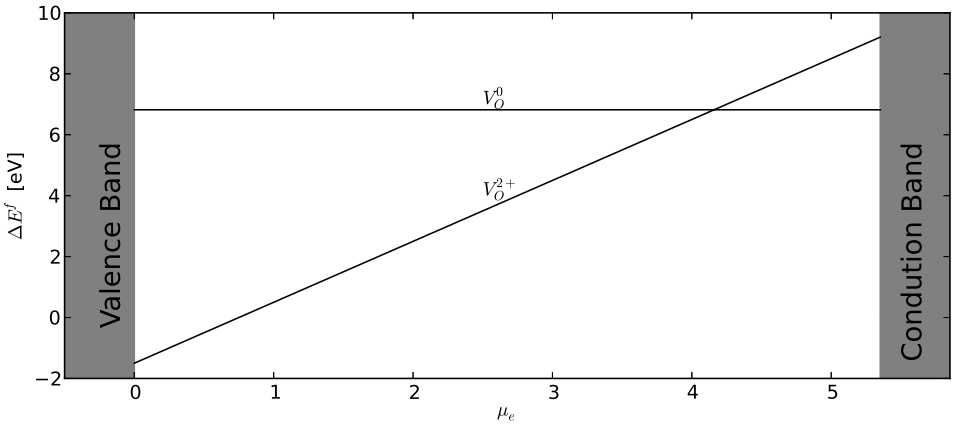

(b)

Figure 7: Formation energy of a neutral and a charged oxygen vacancy within the band gap at concentration $c = 1/81$. The positively charged vacancy is more favorable up to certain value of the electron chemical potential.

creation of a defect. Our $\mathbf{v}^{rel}$ for the vacancy in a 3x3x3 super cell is

$$\mathbf{v}^{rel} = \begin{pmatrix} -3.94 & 0 & 0 \\ 0 & -7.30 & 0 \\ 0 & 0 & -7.30 \end{pmatrix} \text{Å}^3$$

The sum of the tensors eigenvalues is approximately equal to the relaxation volume of the vacancy as it should be. The tensor indicates that $BaZrO_3$ contracts in all directions, but less so along the Zr-V_O-Zr direction so there is an asymmetrical contraction the system undergoes. When the different orientations of the vacancy are taken into account the asymmetry evens out and the contraction is isotropic.

Freedman et al.[48] investigated the long range deformation of $SrTiO_3$ due to a vacancy by calculating the defect strain tensor from the stress induced. The defect strain tensor $\mathbf{\Lambda}$ and $\mathbf{v}^{rel}$ describe the same thing but derived differently. $\mathbf{v}^{rel}$ is calculated from a system that is allowed to relax its size and shape while the system size and shape is kept fixed for $\mathbf{\Lambda}$. Their findings indicate that $SrTiO_3$ expands along the Sr-V_O-Sr direction and contracts in the orthogonal plane in such a way that $SrTiO_3$ experiences a slight expansion when this is averaged over all orientations of the vacancies. This is fundamentally different from what our results for $BaZrO_3$ show.

In figure 8 we observe the local strain around the created oxygen vacancy in the Zr-O plane and in table 5 we've tabulated the change in distance from the vacancy site to the nearest neighbour(NN) shells.

It is interesting that even though the lattice shrinks along the direction of the Zr-V_O-Zr bond the Zr atoms move outwards away from the vacancy, i.e. the Zr-V_O-Zr distance is longer than the undoped Zr-O-Zr. The same is true for the top and bottom oxygen atoms on the in figure 8, those belong to the 4th NN shell. Similar analysis was done by Freedman et al.[48] for the perovskite structured $SrTiO_3$ using a shell model. They used quite a large supercell 14x14x14 and shell potential model for the interactions. Although the strain is qualitatively almost identical to our results the quantitative distortions are notably different. The Sr-V_O-Sr length increases by almost 11% with the introduction of a vacancy while our Zr-V_O-Zr gains only 7%. The other distances behave in a similar manner, i.e. the strain is more exaggerated in the $SrTiO_3$ than in $BaZrO_3$. One anomaly appears in the 4th NN shell, the two oxygen atoms along the Zr-V_O-Zr move closer together, the distance is reduced by 0.5% while the same oxygen atoms in $SrTiO_3$ increase their distance by 1.5%. The other four oxygen atoms in the plane orthogonal to the Zr-V_O-Zr also display different behaviours. The ones in $SrTiO_3$ hardly move at all whilst the $BaZrO_3$ ones increase their distance by 2%.

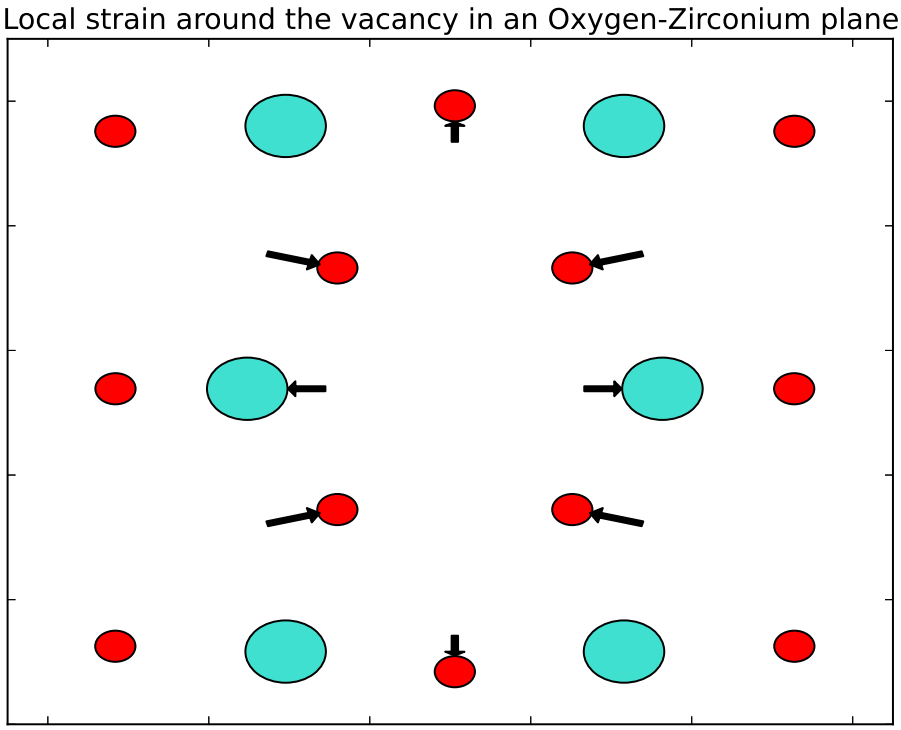

Figure 8: Local strain around the oxygen vacancy(c=1/81). The red circles mark O positions and the blue ones the Zr. All atomic displacements larger than 0.1Å have been exaggerated for illustrative purposes.

Table 5: Local strain. The third column lists distances from an oxygen atom in $BaZrO_3$ to its nearest neighbours in increasing order. The second column shows the distance to the same nearest neighbours from a center of a vacancy created at the oxygen site used for the second column.

-	V_O^{2+} (c=1/81)[Å]	No vacancy[Å]
1NN Zr	2.269	2.117
2NN O	2.793	2.995
3NN Ba	3.059	2.995
4NN O	4.216/4.326	4.235
5NN Zr	4.712	4.735
6NN Ba	5.245	5.187

Because these system share the same structure it is all but natural that they display related behaviour, but as they are two separate materials of course some variation is expected. However it is possible that these variations emerge in part from the fact that our supercell is much smaller and does not imitate the dilute limit accurately. This could be the reason for the less pronounced change in distances that appear in our system since not so far away there are periodically repeated vacancies inducing opposite effects on the atoms. The change in the 4th NN shell behaviour is difficult to explain with respect to finite system size so this might exhibit fundamental differences of these materials.

Freedman et al.[48] investigated the long range deformation of the material due to a vacancy through the elastic dipole tensor. From this tensor the calculate the defect strain tensor with use of elastic compliance tensor. Their findings indicate that $SrTiO_3$ expands along the Sr-V_O-Sr direction and contracts in the orthogonal plane in such a way that $SrTiO_3$ experiences an slight expansion, $\epsilon_c/\delta = 0.001$, when this is averaged over all orientations of the vacancies. This is fundamentally different from what our results for $BaZrO_3$ show. $BaZrO_3$ contracts in all directions, but less along the Zr-V_O-Zr direction. This naturally results in an average contraction $\epsilon_c/\delta = -0.003$.

4.3 Doping and lattice expansion

We investigated the lattice expansion $BaZrO_3$ due to doping by replacing one tetravalent Zr^{4+} by a trivalent atom M^{3+} and allow the cell shape and volume to relax.

Table 6: Expansion according to equation 13 for three different concentrations of V_O^{2+}. The change in lattice constant is averaged over the three orientations.

-	V_O^{2+} (c=1/81)	$3V_O^{2+}$ (c=3/81)	V_O^{2+} (c=1/24)
$\epsilon_{V_O^{2+}}(10^{-3})$	-3.0	-7.9	-9.9

The expansion at a certain dopant concentration x is:

$$\epsilon_M(x) = \frac{a_M(x) - a_{pure}}{a_{pure}} \tag{13}$$

where $a_M(x)$ and a_{pure} are the lattice constants of the doped and un-doped system respectively and the concentration is the sites occupied by M divided by sites available. When we dope the material we also create vacancies. There are twice as many dopants as there are vacancies in order to maintain charge neutrality (one vacancy V^{2+} per two dopant atoms M^{3+} with an effective -1 charge). In table 7 we show $\epsilon_M(x)$ for $BaM_xZr_{1-x}O_{3-x/2}$ with $x = 1/27$ and $x = 1/8$ for a number trivalent dopants M^{3+} in order of their ionic crystal radii. In the table we also include the expansion with effects from vacancies added as $\epsilon = (a_{pure}+(a_M-a_{pure})+0.5(a_V-a_{pure})-a_{pure})/a_{pure}$.

Table 7: Expansion of $BaM_xZr_{1-x}O_{3-x/2}$ as a function of effective ionic radii of the dopant M with coordination number VI.

Dopant	Nd	Eu	Gd	Y	In	Sc	Zr	Ga
Radii(Å)[49]	1.123	1.087	1.078	1.040	0.940	0.885	0.860	0.760
$\epsilon_M(10^{-3})(x = 1/27)$	4.6	4.0	3.5	3.0	1.8	1.2	-	-0.5
$\epsilon_M(10^{-3})(x = 1/8)$	10	-	7.6	6.3	2.1	-0.1	-	-4.3
$\epsilon(10^{-3})(x = 1/27)$	3.1	2.0	1.5	2.5	0.4	-0.3	-	-1.6

We see a correlation between the ionic radii and the expansion of the medium. Ignoring further interactions between the impurities we extrapolate the expansion to higher concentrations (figure 9) and compare it with the expansion calculated at higher concentration. However if we consider the vacancies we see that the expansion at c=3/81 is not simply three times that of c=1/81 rather they decrease non-linearly(table 6). This non-linearity is also apparent in the dopant case for x=1/27

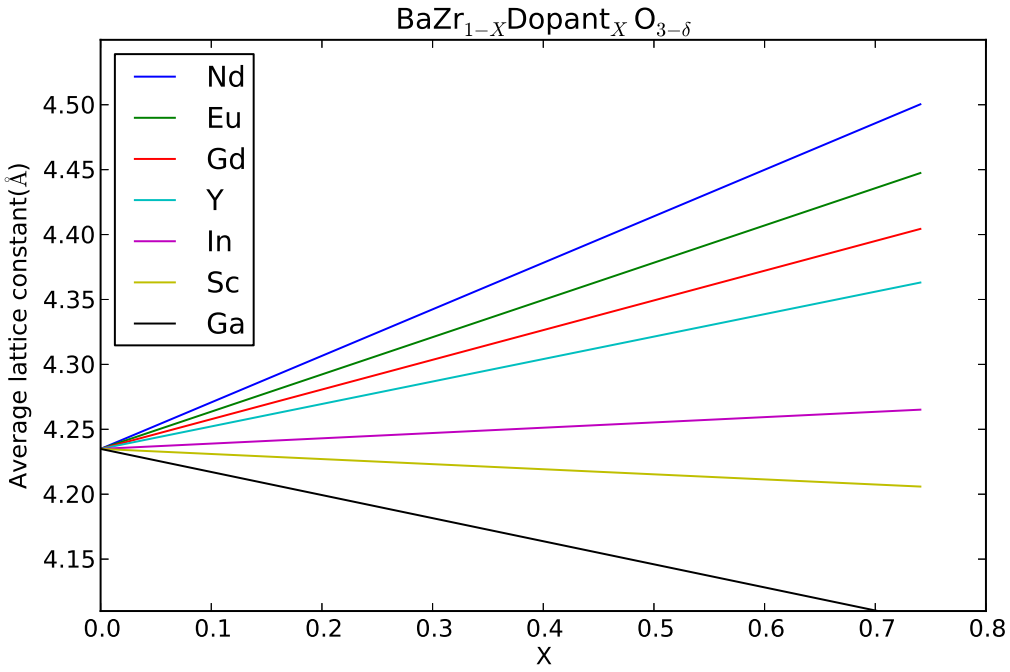

Figure 9: The extrapolated lattice constant calculated from a dopant concentration $x = 1/27$ from DFT calculations. Note that scandium exhibits a negative slope in contrast to having larger ionic radius as given by [49] in table 7.

compared with x=1/8. It is then highly unlikely that the expansion depicted in figure 9 is realistic at higher concentrations than 1/27. Note that Sc doped $BaZrO_3$ is shown to switch from expanding to contracting going from x=1/27 to x=1/8.

In a recent article by Marrocchelli et al.[50] did a combined MD and DFT investigation of the expansion of $Ce^{4+}_{1-x}Ce^{3+}_{x}O_{2-x/2}$ fluorite. They show a linear relationship between the chemical expansion ϵ_c and x for concentrations up to x=0.6. Such a linear model does not seem appropriate for our results. The linear expansion is likely to be caused by the different lattice structure. Trying to model the perovskite expansion in a way similar to what is done in [50] does not lead simple linear expression.

We calculated the expansion due to hydration of $BaIn_xZr_{1-x}O_{3-x/2}$. This we do by adding the change in lattice constant from protonation to the already indium doped system (see figure 10). We interpolated the values closest to 50% doping with $x \approx 0.5$ at 80% protonation. The expansion was calculated 0.75%. This is double what is found experimentally by Knee[51] for the hydrated system, but the expansion

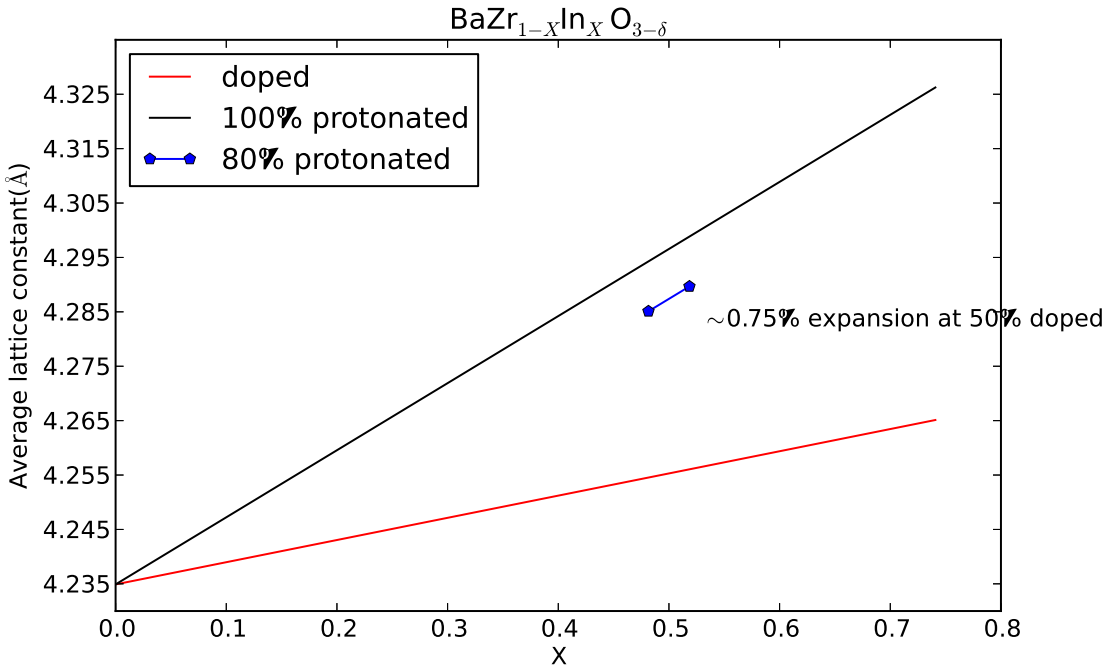

Figure 10: Lattice constant of dry and wet $BaIn_xZr_{1-x}O_{3-x/2}$ as a function of dopant concentration x. The expansion due to hydration is doubly compared to experimentally obtained values from Knee[51].

due to the doping of the system agrees nicely.

4.4 Hydration and oxidation

We calculated the zero pressure reaction enthalpies from eq. 3 for the two processes and the results are shown in table 8. These are calculated using the total energies from a supercell containing 27 primitive cells (135 atoms). What is interesting is that the oxidation reaction switches from being an exothermic reaction to an endothermic one when we use PBE0 rather than PBE while the hydration remains qualitatively the same. An endothermic reaction is more likely to occur in a high temperature environment than at low temperatures as it requires energy. The endothermic PBE0 oxidation might at first glance seem more consistent with an increased conductivity at raised temperatures reported in experiments (figure 2 in [52]) than the exothermic PBE one. However, the conductivity is affected by the hole mobility as well. If the mobility is able to compete with the decreased concentration the conductivity can

	PBE	PBE0
ΔH_{Hydr} [eV](eq. 1)	-0.821	-1.224
ΔH_{Ox} [eV](eq. 2)	-1.008	1.444

Table 8: The zero pressure reaction enthalpies of equation 3 for hydration and oxidation using both GGA and a hybrid functional.

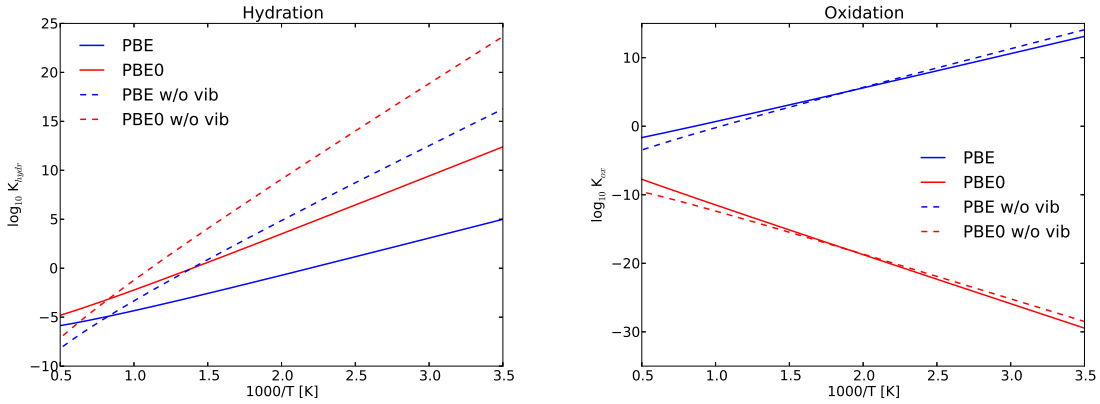

(a) Rate constant for the hydration reaction at $p_{H_2O} = p_0$

(b) Rate constant for the oxidation reaction $p_{O_2} = p_0$

Figure 11: The temperature dependence of the equilibrium rate constants for the two reactions at reference pressure $p = p_0$. There is a clear change in the slope sign between the PBE to PBE0 curve for the oxidation in (b)

increase.

By calculating the equilibrium rate constants we better examine the competition between the reactions. In figure 11 we see the temperature dependance of the rate equilibrium rate constants for the two reactions according to 6. The solid lines show $\log_{10} K$ using ΔG eq. 8 whilst the dashed lines do not include the solid vibrational parts $\Delta\tilde{G}^{vib}(T)$ and $\Delta G^{vib}(T)$. For both the PBE and PBE0 descriptions we have borrowed the PBE vibrational frequencies worked out by [34] to calculate $\Delta\tilde{G}^{vib}(T)$ and $\Delta G^{vib}(T)$. As a result our PBE0 description is not purely PBE0.

The inclusion of $\Delta\tilde{G}^{vib}(T)$ and $\Delta G^{vib}(T)$ for hydration decreases the slope and thus lowers the temperature at which the reaction changes from favoring reactants over products $\log K_{\mathrm{hydr}}(T_0) = 0$. However it does not change the qualitative behavior of the K's. The change from PBE to PBE0 increases the slope and T_0 as suggested by the increased magnitude of the negative reaction enthalpy (table 8). Both of the

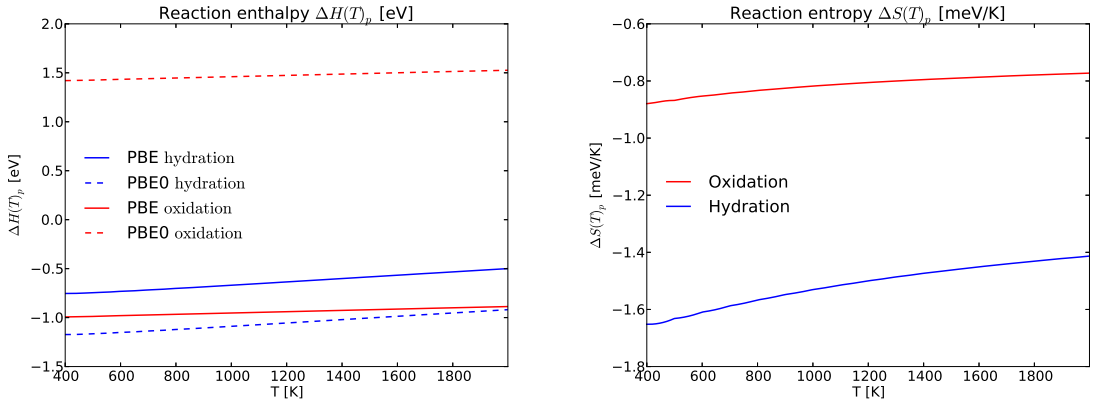

(a) PBE & PBE0 enthalpies for both reactions.

(b) Reaction entropies for both reactions.

Figure 12: The temperature dependent reaction enthalpies and entropies for hydration and oxidation from fitting eq. 7 to each T in eq. 8

curves imply that hydration should occur less frequently as we raise the temperature.

$\Delta\tilde{G}^{vib}(T)$ and $\Delta G^{vib}(T)$ have the same but less pronounced effects on the oxidation rate constants as for the hydration but we see a dramatic change from PBE to PBE0. The positive slope of the PBE rate constant with a definite T_0 warps into a negative slope with seemingly no T_0 (at reference pressure) using PBE0. The qualitative behaviour of the PBE curve is the same as that of the hydration whilst the PBE0 curve implies an increased frequency of oxidation with raised temperature.

Using the approximated T-dependent Gibbs free energy of the reaction 8, we can estimate the temperature dependence of the reaction enthalpy and entropy through linearizing it and reading off the coefficients as

$$\Delta G(p,T) = \Delta H(p,T) - T\Delta S(p,T) \tag{14}$$

In figure 12 we've plotted their temperature dependence using a forward finite difference and solving for $\Delta H(p,T)$ at each T. There is a constant shift in the enthalpy of both reactions going from PBE to PBE0, -0.42 eV and 2.41 eV for hydration and oxidation respectively. Again there is a sign shift for the PBE0. The reaction entropies are calculated using PBE vibrational frequencies so we do not have PBE0 specific entropies. We notice that the similar entropies for both reactions differ in such a way that ΔS_{Hydr} is lower and a bit steeper than ΔS_{Ox}. Our hydration enthalpies are in line with reported experimental values ranging from -1.24 eV to -0.69 eV[3][53][54], the calculated entropies are however significantly lower than the

reported values from -1.29 meV/K to -0.76 meV/K. This is fairly similar to prior results $\Delta H_{\text{Hydr}} = -6.5eV$ and $\Delta S_{\text{Hydr}} = -1.8$ meV/K of Björketun et al.[34] obtained in the same manner and with the same vibrational frequencies for the entropy. Note that the entropy calculated here is closer to the experimental than by Björketun et al. It might be interesting to see if using hybrid functional vibrational frequencies will improve upon this. To the authors knowledge there are no reports on the oxidation enthalpy for $BaZrO_3$.

Finally we've solved for the concentrations by self-consistently fixing μ_e as described in section 3.3 using a program written by Paul Erhart which produces the lovely plots in figure 13. The density of states used was calculated using DFT and the dopant concentration is 10% Y.

In figure 13a we see that with descending temperature from 2000K, c_h and c_{H^+} grow in competition to fill the available vacancies which dwine at the same time. Immediately noticeable is the way in which c_h and c_{H^+} seem have very similar trends throughout the whole temperature range.

The $c_{V_O^{2+}}$ drop in the interval 2000K-650K is roughly $5.6 \cdot 10^{20}$ when c_{H^+} gains about $5.5 \cdot 10^{20}$. For each proton incorporated in the system half a vacancy is filled so the protons can account for close to half of the lost vacancies. The the same applies for the holes, c_h which rises about $1.1 \cdot 10^{20}$ which leaves us with $2.3 \cdot 10^{20}$ lost vacancies unaccounted for.

Throughout the temperature range we see that $c_{Y_{Zr}^-}$ steadily decreases. The Y_{Zr}^- dopants are still there but Y_{Zr} becomes increasingly favorable with declining temperature. The charge difference is compensated by the surplus lost vacancies to keep the charge neutrality condition fulfilled.

At around 600K c_h peaks and begins to die out with the already decreasing $c_{V_O^{2+}}$. A little lower c_{H^+} begins to drop as well. At 300K both c_h and c_{H^+} have fallen roughly 17% of their respective peak values. As with the vacancies at higher temperatures this compensates for the effect the shift in the balance of $c_{Y_{Zr}^-}$ vs. $c_{Y_{Zr}}$ has on the charge neutrality condition. At higher temperatures the decline of $c_{Y_{Zr}^-}$ has been counteracted by a drop in vacancy concentration but at lower temperatures the vacancies are scarce and the protons and holes start to respond.

Since we have holes and protons leaving the system creating vacancies despite the overall decline in $c_{V_O^{2+}}$ there must be a process filling the vacancies. The process of changing the yttrium charge state must be involved.

$$2Y_{Zr}^- + \frac{1}{2}O_2 + V_O^{2+} \leftrightarrow O_O + 2Y_{Zr}$$

The sign shift of the oxidation reaction enthalpy is the qualitative difference in

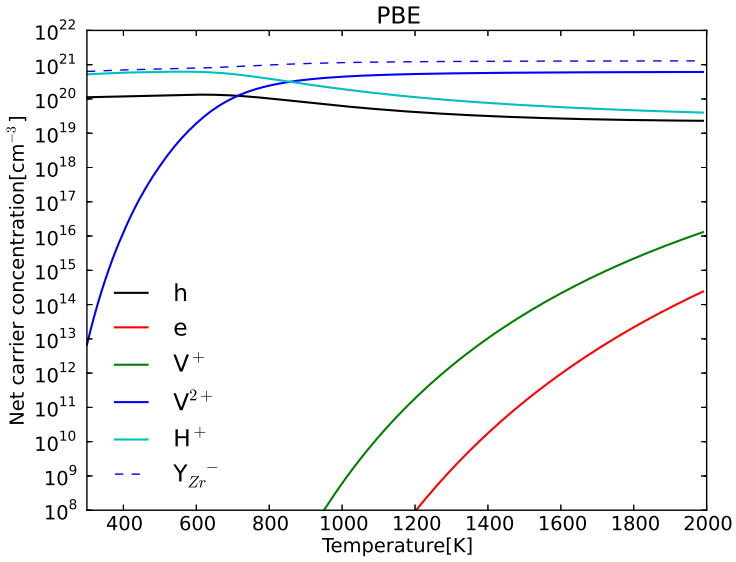

(a) PBE

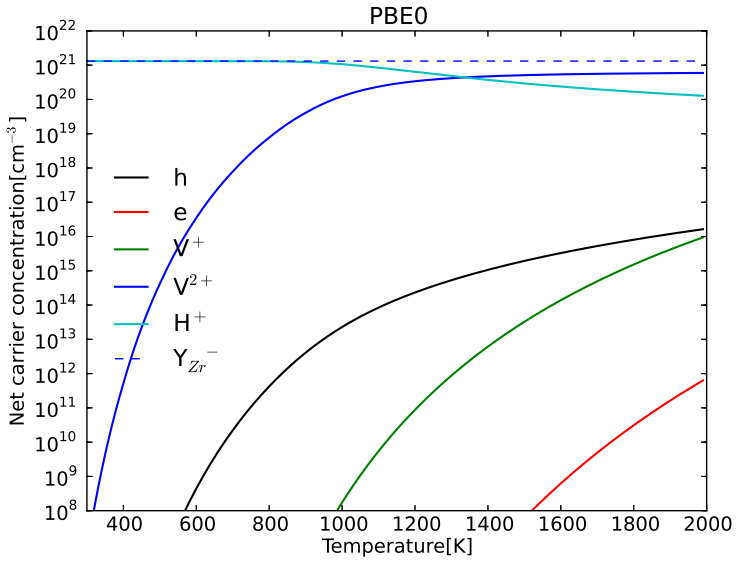

(b) PBE0

Figure 13: Calculated $BaY_{0.1}Zr_{0.9}O_3$ defect concentrations profiles at reference pressures for both PBE and PBE0. The sign change of the reaction enthalpy is evident from the different behavior of the hole concentration (black). In 13a it peaks at around 600K and begins to drop in contrast to the monoclinic behavior in 13b.

the results from the two functionals and we see its effect on c_h in figure 13b. All concentration profiles in 13a and 13b exhibit similar behaviour, although a bit shifted, except c_h which instead of reaching a maximum, keeps growing with increasing temperature in the PBE0 figure 13b.

When the hole concentration begins to drop one would expect the conductivity to drop unless the mobility of the holes increases sufficiently. Bevillion[55] showed that it is possible to have this behaviour if the activation energy for hole migration fulfills the condition $E_a > |\Delta H_{ox}|/4$ where ΔH_{ox} is the oxidation enthalpy per oxygen molecule. The activation energy for the hole migration in yttrium doped $BaZrO_3$ is reported on the order of 0.7-0.9 eV [56][6] which is far greater than our $|\Delta H_{ox}|/4 \approx 0.25$ eV. We conclude that we can not discern which description is more accurate without further knowledge of the temperature dependent mobility.

As mentioned with respect to the formation enthalpies in the beginning of this section, both results can be compatible with the experimental hole conductivity. The PBE0 more directly since the conductivity is proportional to the concentration and PBE more subtly if the mobility adapts.

5 Conclusions

Our pure $BaZrO_3$ calculations support prior calculations that have reported octahedral tilting, however due to the fact that the ground state and tilted state have very similar energies they can probably coexist within a sample. We've seen that the new PAW potentials lead to a slightly more accurate lattice constant than previously obtained with PBE.

A small survey of $BaZrO_3$ electronic structure using both GGA and a hybrid functional approach confirms the excellent improvement of PBE0 on band gap calculations. The DOS changes a substantially between the two methods, most notably the band gap widens, lowering the valence band and raising the conductance band asymmetrically. In addition we calculated the PBE band structure and the formation energy of two differently charged vacancies as a function of the fermi energy within the band gap.

We've also demonstrated that using H_2O molecule for reference calculation instead of O_2 decreases the error caused by overestimated binding energies of the molecules by 40%. This should result in a more accurate formation energy for $BaZrO_3$.

We've noticed discrepancies between the local environment of an doubly positive oxygen vacancy in our $BaZrO_3$(DFT) and a $SrTiO_3$ shell model simulation. Although the qualitative behaviour of the nearest neighbours is the same (with some

exceptions) in both systems the $BaZrO_3$ environment seems to be more rigid. We conclude that the more rigid behaviour of our system might be an artifact of the limited size and periodicity of the system, however some of the more irregular discrepancies probably are not.

The most notable large scale difference between the systems is that $BaZrO_3$ contracts due to a vacancy whereas $SrTiO_3$ slightly expands. From this we see that filling vacancies will cause $BaZrO_3$ to expand.

Our data on the expansion effects of vacancies and dopants do not exhibit the same linear behaviour as the fluorite structured $Ce^{4+}_{1-x}Ce^{3+}_{x}O_{2-x/2}$. By adding lattice effects from vacancies, dopants and protons separately we've tried to imitate the expansion caused by first doping and then hydrating $BaZrO_3$. Assuming a linear behaviour of the expansion up to $BaZr_{0.5}In_{0.5}O_{2.75}$ and adding lattice effects from vacancies, dopants and protons separately, we've tried imitate the expansion caused by first doping and then hydrating. We fail to reproduce the experimental hydration expansion measured by others. But the expansion due to doping is not far off.

The zero pressure hydration enthalpy and the temperature dependent enthalpy calculated from the Gibbs energy seem in line with experimental data, both for PBE and PBE0. The entropy which uses only PBE data is severely underestimated but less so than prior calculations using similar methods. Further work could explore if a full PBE0 description would improve this further.

The zero pressure enthalpy for oxidation is positive when calculated with PBE0 (hybrid) in contrast to the negative enthalpy of PBE (GGA). This drastic change is evident throughout further comparison of the equilibrium rate constants for the oxidation and the defect concentrations profiles using PBE and PBE0.

The PBE0 results describe an endothermic oxidation that becomes more frequent with raised temperature. The PBE0 concentration of holes grows with increasing temperature. This agrees well with experiments that report an increased electrical conductivity at elevated temperatures, since the electron hole concentration is directly related to the oxidation.

The PBE results describe an exothermic oxidation with a growing concentration of holes up to about 620K. When the temperature is raised further the concentration of holes drops dramatically.

Despite the drop in hole concentration the PBE results do not necessarily contradict the experimental evidence of increased electrical conductivity at raised temperature. As long as the oxidation enthalpy fulfills the condition $E_a > |\Delta H_{ox}|/4$ (demonstrated by [55]) the conductivity rises in spite of the lowered concentration of the charge carrier. In order to learn whether PBE or PBE0 is more accurate we need more information about the hole mobility.

Of course the concentration profiles examined here do not include all possible defects but we believe we have included the most important ones. However, other defects might play an important role and a more detailed study might shed some new light on the oxidation process.

References

[1] KD Kreuer. Proton-conducting oxides. *Annual Review of Materials Research*, 33(1):333–359, 2003.

[2] P. S. Dobal, A. Dixit, R. S. Katiyar, Z. Yu, R. Guo, and A. S. Bhalla. Micro-raman scattering and dielectric investigations of phase transition behavior in the $BaTiO_3$–$BaZrO_3$ system. *Journal of Applied Physics*, 89(12):8085–8091, 2001.

[3] T. Schober and H.G. Bohn. Water vapor solubility and electrochemical characterization of the high temperature proton conductor $BaZr_{0.9}Y_{0.1}O_{2.95}$. *Solid State Ionics*, 127(3–4):351 – 360, 2000.

[4] Emiliana Fabbri, Lei Bi, Hidehiko Tanaka, Daniele Pergolesi, and Enrico Traversa. Chemically stable Pr and Y Co-doped barium zirconate electrolytes with high proton conductivity for intermediate-temperature solid oxide fuel cells. *Advanced Functional Materials*, 21(1):158–166, 2011.

[5] K.D Kreuer. Aspects of the formation and mobility of protonic charge carriers and the stability of perovskite-type oxides. *Solid State Ionics*, 125(1–4):285 – 302, 1999.

[6] Hans G. Bohn and Tilman Schober. Electrical conductivity of the high-temperature proton conductor $BaZr_{0.9}Y_{0.1}O_{2.95}$. *Journal of the American Ceramic Society*, 83(4):768–772, 2000.

[7] J. Robertson. Band offsets of wide-band-gap oxides and implications for future electronic devices. *Journal of Vacuum Science & Technology B: Microelectronics and Nanometer Structures*, 18:1785, 2000.

[8] Fumitada Iguchi, Takehisa Yamada, Noriko Sata, Takao Tsurui, and Hiroo Yugami. The influence of grain structures on the electrical conductivity of a $BaZr_{0.95}Y_{0.05}O_3$ proton conductor. *Solid State Ionics*, 177(26–32):2381 – 2384, 2006. Solid State Ionics 15: Proceedings of the 15th International Conference on Solid State Ionics, Part II.

[9] Ante Bilić and Julian Gale. Ground state structure of $BaZrO_3$: A comparative first-principles study. *Physical Review B*, 79(17):1–9, 2009.

[10] Yoshihiro Yamazaki, Chih-Kai Yang, and Sossina M. Haile. Unraveling the defect chemistry and proton uptake of yttrium-doped barium zirconate. *Scripta Materialia*, 65(2):102 – 107, 2011. Viewpoint set no. 48: Solid Oxide Fuel Cells.

[11] Max Born and Robert Oppenheimer. Zur Quantentheorie der Molekeln. *Annalen der Physik*, 84:457–484, 1927.

[12] P. Hohenberg and W. Kohn. Inhomogeneous electron gas. *Phys. Rev.*, 136:B864–B871, Nov 1964.

[13] W. Kohn and L. J. Sham. Self-consistent equations including exchange and correlation effects. *Phys. Rev.*, 140:A1133–A1138, Nov 1965.

[14] D. M. Ceperley and B. J. Alder. Ground state of the electron gas by a stochastic method. *Phys. Rev. Lett.*, 45:566–569, Aug 1980.

[15] A. D. Becke. Density-functional exchange-energy approximation with correct asymptotic behavior. *Phys. Rev. A*, 38:3098–3100, Sep 1988.

[16] Chengteh Lee, Weitao Yang, and Robert G. Parr. Development of the colle-salvetti correlation-energy formula into a functional of the electron density. *Phys. Rev. B*, 37:785–789, Jan 1988.

[17] John P. Perdew and Yue Wang. Accurate and simple analytic representation of the electron-gas correlation energy. *Phys. Rev. B*, 45:13244–13249, Jun 1992.

[18] John P. Perdew, Kieron Burke, and Matthias Ernzerhof. Generalized gradient approximation made simple. *Phys. Rev. Lett.*, 77(18):3865–3868, October 1996.

[19] K. Capelle. A bird's-eye view of density-functional theory. *eprint arXiv:cond-mat/0211443*, November 2002.

[20] Joachim Paier, Robin Hirschl, Martijn Marsman, and Georg Kresse. The Perdew–Burke–Ernzerhof exchange-correlation functional applied to the G2-1 test set using a plane-wave basis set. *The Journal of Chemical Physics*, 122(23):234102, 2005.

[21] John P. Perdew, Kieron Burke, and Yue Wang. Generalized gradient approximation for the exchange-correlation hole of a many-electron system. *Phys. Rev. B*, 54:16533–16539, Dec 1996.

[22] John P. Perdew and Mel Levy. Physical content of the exact Kohn-Sham orbital energies: Band gaps and derivative discontinuities. *Phys. Rev. Lett.*, 51:1884–1887, Nov 1983.

[23] L. J. Sham and M. Schlüter. Density-functional theory of the energy gap. *Phys. Rev. Lett.*, 51:1888–1891, Nov 1983.

[24] L. J. Sham and M. Schlüter. Density-functional theory of the band gap. *Phys. Rev. B*, 32:3883–3889, Sep 1985.

[25] Stefan Kurth, John P. Perdew, and Peter Blaha. Molecular and solid-state tests of density functional approximations: LSD, GGAs, and meta-GGAs. *International Journal of Quantum Chemistry*, 75(4-5):889–909, 1999.

[26] A.D. Becke. Density-functional thermochemistry. III. the role of exact exchange. *The Journal of Chemical Physics*, 98:5648, 1993.

[27] J. Harris. Adiabatic-connection approach to Kohn-Sham theory. *Phys. Rev. A*, 29:1648–1659, Apr 1984.

[28] A.D. Becke. Density-functional thermochemistry. IV. a new dynamical correlation functional and implications for exact exchange mixing. *The Journal of Chemical Physics*, 104:1040–1045, 1996.

[29] John P. Perdew, Matthias Ernzerhof, and Kieron Burke. Rationale for mixing exact exchange with density functional approximations. *J. Chem. Phys.*, 105(22):9982–9985, 1996.

[30] Carlo Adamo and Vincenzo Barone. Toward reliable density functional methods without adjustable parameters: The PBE0 model. *The Journal of Chemical Physics*, 110(13):6158–6170, 1999.

[31] Felix Bloch. Über die Quantenmechanik der Elektronen in Kristallgittern. *Zeitschrift für Physik A Hadrons and Nuclei*, 52(7):555–600, July 1929.

[32] Computer code VASP. http://www.vasp.at/.

[33] M Leslie and N J Gillan. The energy and elastic dipole tensor of defects in ionic crystals calculated by the supercell method. *Journal of Physics C: Solid State Physics*, 18(5):973, 1985.

[34] Mårten E. Björketun, Per G. Sundell, and Göran Wahnström. Structure and thermodynamic stability of hydrogen interstitials in $BaZrO_3$ perovskite oxide from density functional calculations. *Faraday Discuss.*, 134:247–265, 2007.

[35] Neil W. Ashcroft and David N. Mermin. *Solid State Physics*. Thomson Learning, Toronto, 1 edition, January 1976.

[36] J. Muscat, A. Wander, and NM Harrison. On the prediction of band gaps from hybrid functional theory. *Chemical Physics Letters*, 342(3):397–401, 2001.

[37] Peter Atkins and Julio De Paula. *Physical Chemistry*. Oxford University Press, 8Rev Ed edition, March 2006.

[38] W. Pies and A. Weiss. *Landolt-Börnstein: Numerical Data and Functional Relationships in Science and Technology*, edited by K.-H. Hellweg and A. M. Hellwege, New Series, Group III, Vols. 7b1 (Springer, Berlin, 1975) and 7e (Springer, Berlin, 1975).

[39] Per G. Sundell, Mårten E. Björketun, and Göran Wahnström. Thermodynamics of doping and vacancy formation in $BaZrO_3$ perovskite oxide from density functional calculations. *Phys. Rev. B*, 73:104112, Mar 2006.

[40] A. R. Akbarzadeh, I. Kornev, C. Malibert, L. Bellaiche, and J. M. Kiat. Combined theoretical and experimental study of the low-temperature properties of $BaZrO_3$. *Phys. Rev. B*, 72:205104, Nov 2005.

[41] Joseph W. Bennett, Ilya Grinberg, and Andrew M. Rappe. Effect of symmetry lowering on the dielectric response of $BaZrO_3$. *Phys. Rev. B*, 73:180102, May 2006.

[42] Francesco Giannici, Mona Shirpour, Alessandro Longo, Antonino Martorana, Rotraut Merkle, and Joachim Maier. Long-range and short-range structure of proton-conducting Y:$BaZrO_3$. *Chemistry of Materials*, 23(11):2994–3002, 2011.

[43] Maria A. Gomez, Mary A. Griffin, Saryu Jindal, Kristin D. Rule, and Valentino R. Cooper. The effect of octahedral tilting on proton binding sites and transition states in pseudo-cubic perovskite oxides. *The Journal of Chemical Physics*, 123(9):094703, 2005.

[44] Mårten Björketun. *Hydrogen in oxides: a density-functional study of thermodynamic and kinetic aspects*. PhD thesis, Chalmers University of Technology, Göteborg, Sweden, 2007.

[45] Tsuneo Matsui. Thermodynamic properties of ternary barium oxides. *Thermochimica Acta*, 253(0):155 – 165, 1995. Thermal Measurements, A Selection of Papers Presented at the International and III Sino-Japanese Symposium on Thermal Measurements.

[46] M. W. Chase. Janaf thermochemical tables 3rd ed. *(American Chemical Society and the American Institute of Physics, New York)*, 1986.

[47] Scott A. Centoni, Babak Sadigh, George H. Gilmer, Thomas J. Lenosky, Tomás Díaz de la Rubia, and Charles B. Musgrave. First-principles calculation of intrinsic defect formation volumes in silicon. *Phys. Rev. B*, 72:195206, Nov 2005.

[48] Daniel A. Freedman, D. Roundy, and T. A. Arias. Elastic effects of vacancies in strontium titanate: Short- and long-range strain fields, elastic dipole tensors, and chemical strain. *Phys. Rev. B*, 80:064108, Aug 2009.

[49] R. D. Shannon. Revised effective ionic radii and systematic studies of interatomic distances in halides and chalcogenides. *Acta Crystallographica Section A*, 32(5):751–767, September 1976.

[50] Dario Marrocchelli, Sean R. Bishop, Harry L. Tuller, and Bilge Yildiz. Understanding chemical expansion in non-stoichiometric oxides: Ceria and zirconia case studies. *Advanced Functional Materials*, 22(9):1958–1965, May 2012.

[51] Christopher Knee. personal communication, 2012.

[52] P. Erhart and K. Albe. Modeling the electrical conductivity in $BaTiO_3$ on the basis of first-principles calculations. *Journal of Applied Physics*, 104(4):044315 – 044315–8, January 2012.

[53] K.D. Kreuer, St. Adams, W. Műnch, A. Fuchs, U. Klock, and J. Maier. Proton conducting alkaline earth zirconates and titanates for high drain electrochemical applications. *Solid State Ionics*, 145(1–4):295 – 306, 2001. Proceedings of the 10th International Conference on Solid State Protonic Conductors.

[54] Bodo Groß, Jurgen Engeldinger, Dieter Grambole, Folker Herrmann, and Rolf Hempelmann. Dissociative water vapor absorption in $BaZr_{0.85}Y_{0.15}O_{2.925}/H_2O$: pressure-compositions isotherms in terms of Fermi-Dirac statistics. *Phys. Chem. Chem. Phys.*, 2:297–301, 2000.

[55] Emile Bévillon, Guilhem Dezanneau, and Grégory Geneste. Oxygen incorporation in acceptor-doped perovskites. *Phys. Rev. B*, 83:174101, May 2011.

[56] Katsuhiro Nomura and Hiroyuki Kageyama. Transport properties of $Ba(Zr_{0.8}Y_{0.2})O_{3-\delta}$ perovskite. *Solid State Ionics*, 178(7–10):661 – 665, 2007. 13th Solid State Proton Conductors Conference.

CHALMERS UNIVERSITY OF TECHNOLOGY
SE 412 96 Göteborg, Sweden
Phone: + 46 - (0)31 772 10 00
Web: www.chalmers.se